GeoScienceWorld
Lithosphere
Volume 2022, Article ID 9260593, 14 pages
https://doi.org/10.2113/2022/9260593

Lithosphere

Research Article

Comprehensive Experimental Study on the Gas Breakthrough Pressure and Its Implication for the Reservoir Performance

Hengrong Zhang,[1,2] **Lizhi Xiao**,[1] **Min Wang**,[3] **Xinmin Ge**,[4] **Xiangyang Hu**,[2] **and Wei Tan**[2]

[1]*China University of Petroleum (Beijing), Beijing, China*
[2]*CNOOC Limited, Zhanjiang, China*
[3]*Research Institute of Exploration and Development of Shengli Oilfield, Sinopec, Dongying, China*
[4]*China University of Petroleum (East China), Qingdao, China*

Correspondence should be addressed to Hengrong Zhang; 176035051@qq.com and Lizhi Xiao; xiaolizhi@cup.edu.cn

Received 13 July 2022; Revised 3 November 2022; Accepted 25 November 2022; Published 14 December 2022

Academic Editor: Xiangyang Xie

It is challenging to interpret the gas breakthrough mechanisms, controlling factors, and its relationships with the reservoir parameters for unconventional reservoirs such as the gas shale, due to the accumulation characteristics of source-reservoir integration. Take the typical marine shale gas of the B field for example, we use the step-by-step (SBS) test to measure the gas breakthrough pressure of the water saturated shales, and investigate the influential factors such as the pore size distribution, mineral composition, and organic geochemical properties. Moreover, the implication of the gas breakthrough capability for the reservoir quality such as the porosity, permeability, the gas content, and the gas occurrence state are addressed. Based on our work, it is observed that the gas breakthrough capability in shale is influenced by many factors. Generally, the gas breakthrough pressure is positively with the amount of ductile minerals such as the clay and the plagioclase, but negatively with the amount of brittle minerals such as the quartz. In addition, the gas breakthrough pressure is decreased with the increase of the pore radius and the specific surface areas. What is more, the influences of geochemical properties on the gas breakthrough capability should not be neglected. Due to the development of organic pores in the kerogen, the gas breakthrough pressure is found to decrease with the increase of the total organic carbon content (TOC) and the residual carbon content (RC). The breakthrough pressure can be used as the significant parameter to indicate the reservoir quality of the shale gas. It is shown that the breakthrough pressure is inversely with the porosity, permeability, the total gas content, and the adsorbed gas content. It is practical and meaningful to measure and estimate the breakthrough pressure for the formation evaluation in shale gas reservoirs.

1. Introduction

The gas breakthrough pressure is defined as the minimal capillary pressure for gas (the non-wetting phase) to flow continuously in brine saturated porous rock, which is also termed as the threshold pressure, the displacement pressure, and the critical pressure. It acts as one of the most important parameter for the formation evaluation of hydrocarbon reservoirs since it controls the caprock sealing efficiency and reflects the fluid accumulation and migration behavior [1–4]. It is also imperative for many geological fields such as the carbon dioxide (CO_2) sequestration, the enhanced oil recovery (EOR), the high-level nuclear waste underground disposal, and the landfill final cover [5–17].

There are comprehensive results on the laboratory measurement and well logging evaluation of the gas breakthrough pressure for conventional reservoirs with simple reservoir-seal assemblage, and mainly focused on the mudstone and shale caprock, frequently occurred over the oil and sections [18–23]. However, the gas breakthrough mechanism and fluid accumulation is more complicated in unconventional reservoirs such as the gas shale. Due of the near source accumulation and the source-

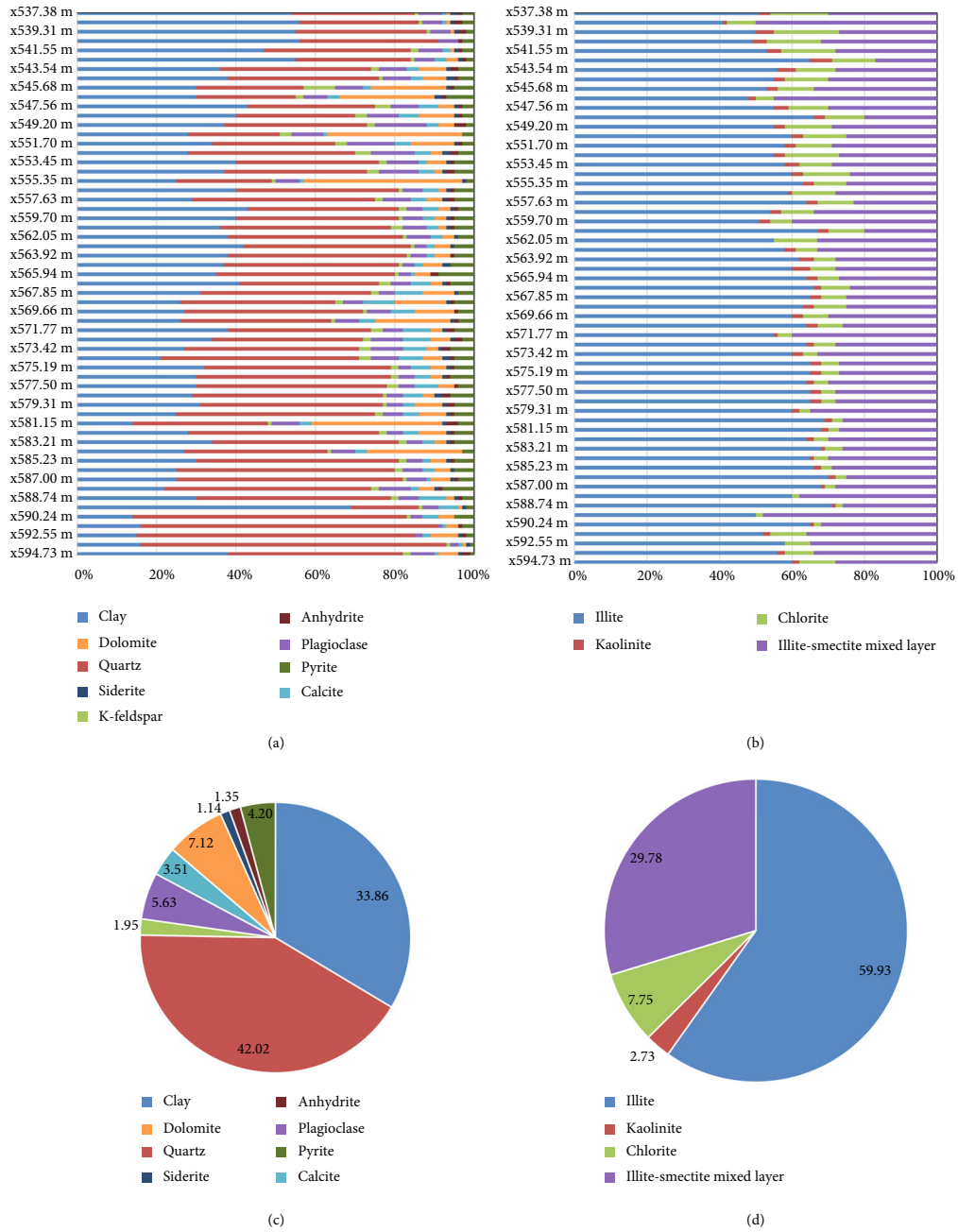

Figure 1: The X-ray diffraction (XRD) data of the Longmaxi Formation in Y-XX well. (a) Minerals. (b) Clays. (c) Average value of minerals. (d) Relative average value of clays.

reservoir integration features [24–26], it is difficult to determine the gas breakthrough pressure by conventional regressions of geophysical logging data such as the resistivity, acoustic velocity, the density, and the natural gamma ray intensity [27–32]. For a better understanding on the breakthrough pressure of the gas shale, it is imperative to conduct the laboratory study to investigate the influential factors and the controlling factors on the gas breakthrough capability as well as its correlations with the reservoir parameters including the porosity and the gas content.

In this study, we measured the gas breakthrough pressure on selected samples from the A block of the B shale gas field in southwest China by the step-by-step (SBS) test under the reservoir conditions. In additional, the twin samples are also collected to get the petrophysical and petrological information such as the mineral compositions, the pore size distributions, the geochemical analysis, and the gas contents. The main aim is to characterize the gas breakthrough pressure and its correlations with petrologic and petrophysical characteristics and to further reveal its implications for the reservoir quality of the gas shale.

2. Materials and Experiments

2.1. Geological Setting and Petrologic Characteristics. The A block of the B shale gas field is located in eastern Sichuan Basin of southwest China. It is a typical shale gas reservoir covering an area of approximately 1200 km^2. The sedimentary environment is dominated by deep-shallow water shelf subfacies deposits with occasional low-density turbidity and carbonate debris flow. The prominent gas-bearing shales are distributed from the late Ordovician Wufeng Formation to the early Silurian Longmaxi Formation, with the buried depth ranges from ×300 m to ×595 m in exploration wells [33]. The upper and middle part to the Longmaxi Formation are developed with a suite of light grey-grey mudstones of shallow-water shelf facies, and a suite of grey-dark grey muddy siltstone, respectively. Whereas, the lower part of the Longmaxi Formation is developed with a suite of dark grey-black carbonaceous mudstone and shale of deep water shelf facies [34–36].

Figure 1 shows the mineral and clay composition and their contents of the Longmaxi Formation in Y-XX, an exploration well in the A area. It is clear that the formation is dominated by the quartz and the clay, with an average value of 34% and 42%, respectively, followed by the dolomite and the plagioclase. Moreover, the clay is generally composed by the illite and the illite-smectite mixed layer. As we known, the clay is strongly correlated with the adsorbed methane since it provides the favorable storage space for the gas. Inversely, the brittleness mineral such as the quartz is favorable for the gas production. We also observed that the pyrite is commonly presented in the formation, revealing the sedimentary environment is positive to the preservation of the kerogen and organic matters [37]. However, it is unfavorable for petrophysical logging operations and formation evaluation since it is conductive and paramagnetic, the measured resistivity and nuclear magnetic resonance intensity may be reduced. There is no clear correlation between the depth and the mineral contents, showing strong vertical heterogeneity of the mineral's distribution.

Figure 2 shows the typical thin sections of the Longmaxi Formation in Y-XX well. The lithology is mainly composed by the silty carbonaceous shale (Figure 2(a)) and the silty carbonaceous mudstone (Figure 2(b)), which is difficult to be discriminated from the conventional geophysical well logging response. The grain size is generally lower than 0.03 mm and inhomogeneous distributed. The linear beddings formed by the acicular muscovite, the siltstone, and the dolomite are commonly developed. Some carbonaceous shales are developed with spherical-like siderites and dispersed siltstones (Figure 2(c)), coming into being the well-developed laminas with the dolomite and the acicular muscovite. A small amount of crystal tuffs is also observed, as is seen in Figure 2(d). The crystal fragment (mostly are the biotite and the quartz) content is as high as 30%, the other parts are the clay altered from the volcanic dust (account for 64%) and the crystalline grained pyrite (account for 6%). The mineral information inferred from the thin section is generally agreed with the XRD analysis.

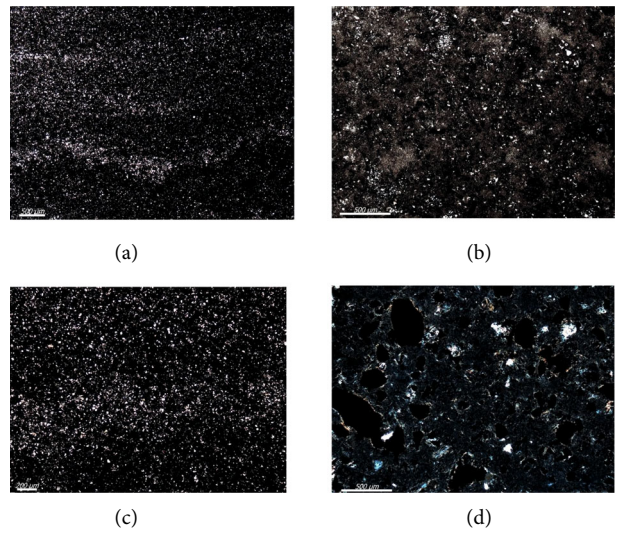

FIGURE 2: Typical thin section images of the Longmaxi Formation in Y-XX well. (a) The silty carbonaceous shale at the depth of ×558.79 m. (b) The silty carbonaceous mudstone at the depth of ×537.38 m. (c) The siderite-bearing silty carbonaceous shale at the depth of ×567.85 m. (d) The crystal tuff at the depth of ×571.77 m.

Figure 3 gives the scanning electron microscopy (SEM) images of the silty carbonaceous mudstone at the depth of ×537.38 m. Compared with the thin section, the SEM images provide more detailed information on the pore space and the pore distributions. The sample is polished by the argon ion before the experiment. It is seen that the sample is mostly developed cellular distributed with round and elliptic organic pores. The pore radius is widely distributed, ranging from the nanoscale to the micron-scale. Moreover, the clay intracrystalline pores, the dissolved pores, and the pyrite intracrystalline pores and the microfractures are also observed. These pores provide favorable space for the adsorption and the storage of the methane.

Figures 4(a) and 4(b) give the total organic carbon content (TOC), the sulfur content (S), the porosity, and the permeability from core analysis at different depths in the Longmaxi formation of Y-XX well. The TOC is generally increased with the increase of the depth and reaches the maximal values at approximate ×585 m. The trend for the porosity and the permeability is similar to the TOC, indicating that the reservoir quality is improved by the TOC (see in Figures 4(c) and 4(d)). The potential reason is that the kerogen is well developed with the organic pores, increasing the porosity and the permeability. Similar relationships were also observed by other researchers [38–41].

2.2. The SBS Gas Breakthrough Pressure Experiment. Compared with the mercury injection porosimetry (MIP) method and the residual capillary pressure (RCP) method, the SBS method is recognized as the direct technique for obtaining the gas breakthrough pressure [5, 30, 42, 43]. Moreover, the SBS method can be performed at reservoir conditions (high pressure and elevated temperature) to simulate the in situ two-phase flow, providing accurate and reliable results [1, 8, 43, 44]. In this study, the gas

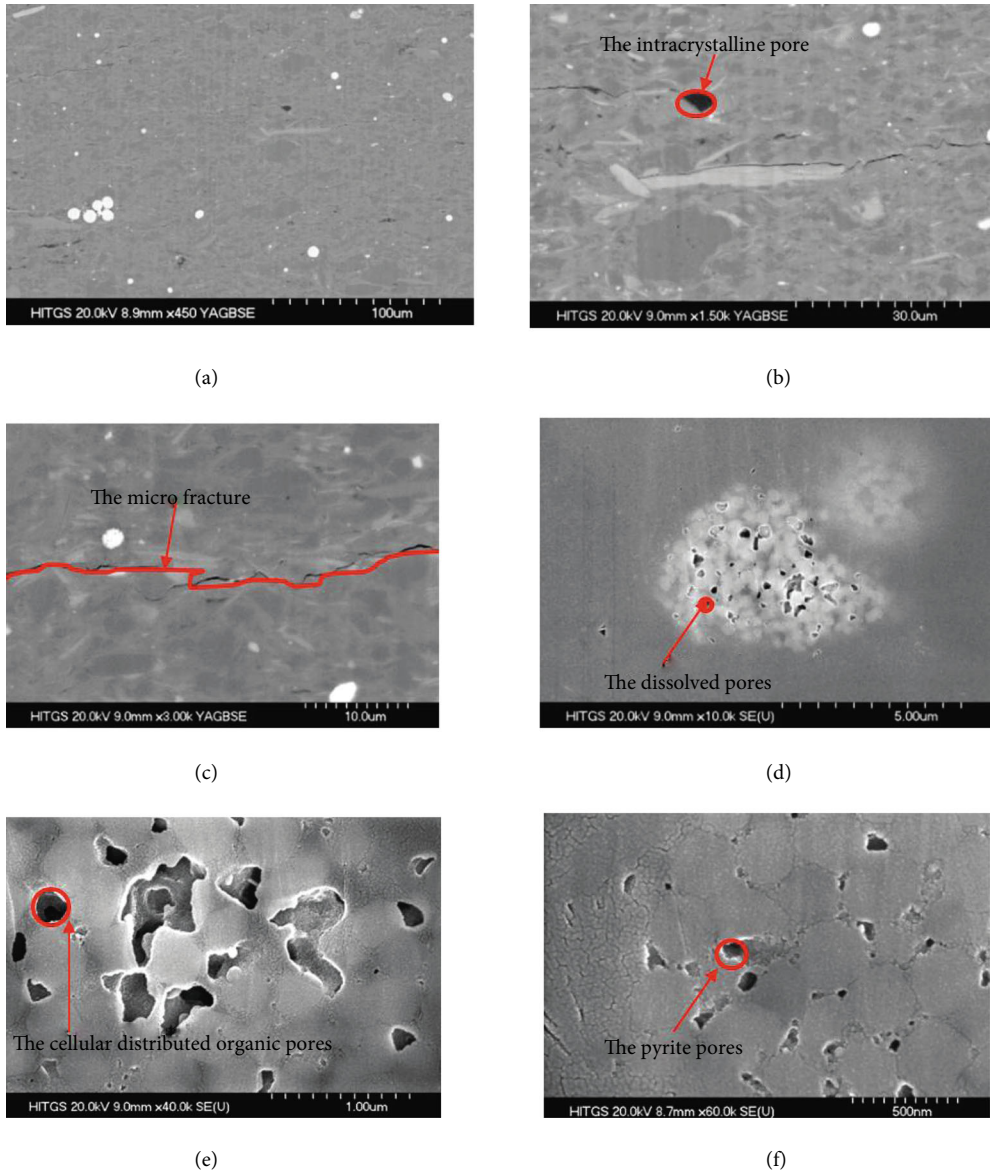

Figure 3: SEM images of different magnifications for the silty carbonaceous mudstone at the depth of ×537.38 m.

breakthrough pressure experiment is conducted by the SBS method, according to China Oil and Gas Industry Standards of "Determination method of gas breakthrough pressure in rock: SY/T5748-2013" [45]. The schematic of the experimental apparatus is shown in Figure 5. It is performed under the confining pressure of 65 MegaPascals (MPa) and the temperature of 90°C. The experimental procedure is expressed as follows. (1) Collect and reshape these samples into cylindrical plugs, and clean them to remove the pore fluids and drilling muds. (2) Measure the porosity and permeability by the helium method and saturate them with the salinity water. (3) Put into the experimental system and elevate the confining pressure and temperature to the assumed values of 65 MPa and 90°C. (4) Monitor the pressure and temperature to make sure the stability of the equipment at last 30 minutes. (5) Adjust the inlet pressure to proper value according to the initial pressure difference defined in Table 1 and the outlet pressure. (6) Increase the inlet pressure to conduct the gas pressure measurement according to the pressure gap and time duration defined in Table 2. (7) Monitor the bubble of the outlet to determine the breakthrough condition. (8) Record the pressure difference between the inlet and the outlet as the gas breakthrough pressure when the bubble is escaped continuously and evenly. Meanwhile, the XRD analysis, the Rock-Eval pyrolysis, the high-pressure adsorption isothermal, and the high pressure MIP are also conducted for twin samples with the same depth. Consequently, the petrological information such as the mineral and clay contents, the petrographic information, the petrophysical information, the geochemical information, and the gas occurrence state and its content can be achieved conveniently. In our experiments, the MIP measurement was performed by the Micrometrics Autopore TM IV 9505 (Micromeritics Instruments Corporation, Norcross,

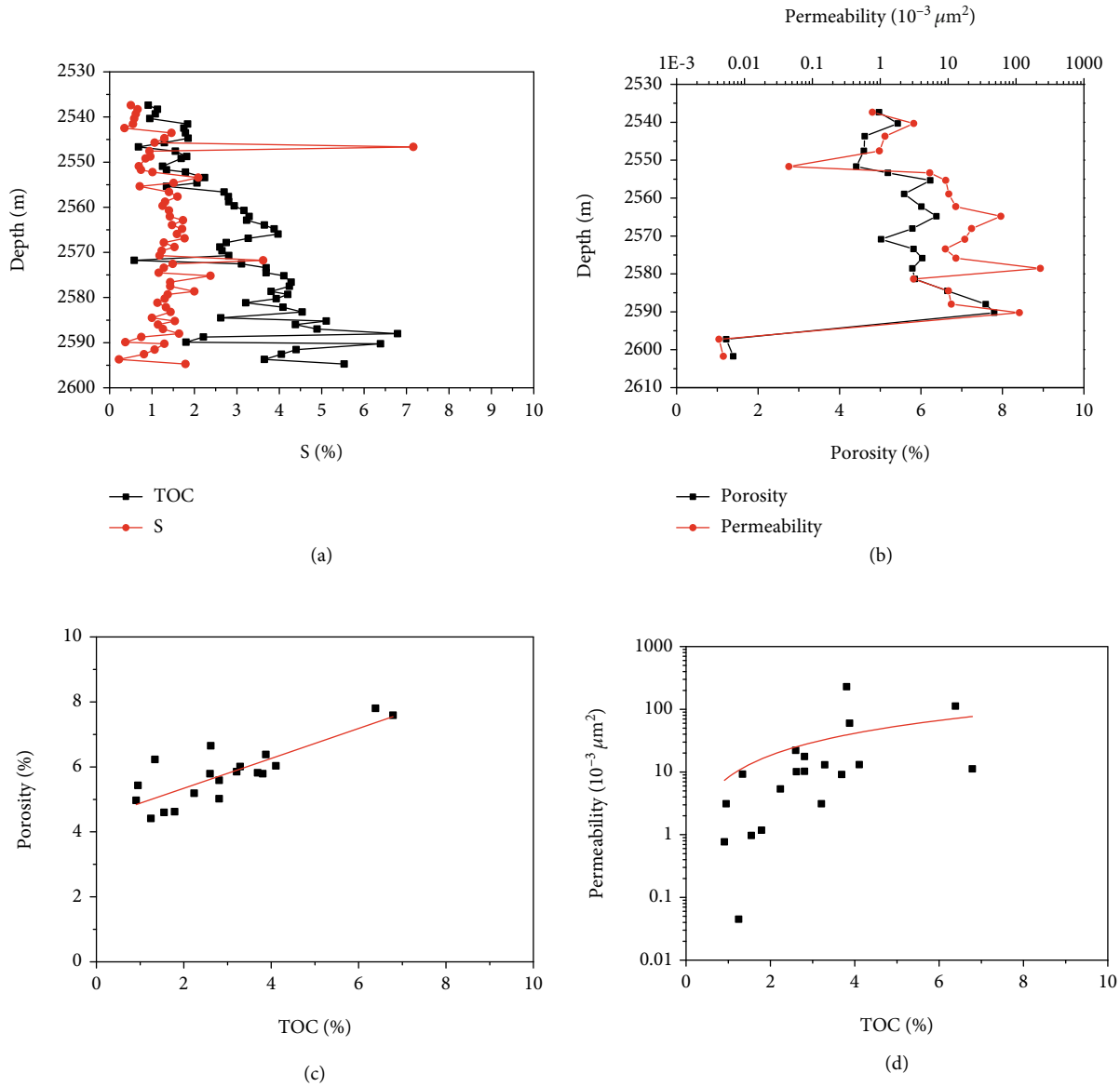

Figure 4: The TOC, the S, the porosity, and the permeability of the Longmaxi Formation in Y-XX well. (a) TOC and S. (b) Porosity and permeability. (c) TOC and porosity. (d) TOC and permeability.

USA), and the nitrogen adsorption measurement was performed with the QuadraSorb SI (Quantachrome Instruments, Boynton Beach, USA) and the accessional software QuadraWin version 5.04. The experiment details can be seen in our previous publication [37].

3. Results and Analysis

3.1. Relationship with the Pore Parameters. According to the International Union of Pure and Applied Chemistry (IUPAC), the pores can be classified based on their radius as micropores (pore radius less than 1 nm), mesopores (pore radius between 1 nm and 25 nm), and macropores (pore radius greater than 25 nanometer (nm)) [46, 47]. The maximal entry pressure of the MIP experiment can be reached to 200 MPa (corresponding to the pore radius of 3.8 nm), both the macropores (>25 nm) and some mesopores (3.8 nm~25 nm) can be obtained. As is shown in Figures 6(a)–6(c), the breakthrough pressure is positively correlated with the capillary pressure (Pc) when the mercury saturation reaches 10% ($Pc_{10\%}$) and 30%($Pc_{30\%}$), and negatively correlated with the mean pore radius (R_{MICP}), revealing that the gas is easier to transport and breakthrough in larger pores than small pores. The nitrogen (N_2) adsorption experiments at the temperature of -196.15°C are also conducted on these samples to get the entire pore size distribution of mesopores. The pore radius distribution is obtained by the Barrett-Joyner-Halenda (BJH) theory (R_{BJH}). As is seen in Figure 6(d), the mean pore radius ranges from 1.4 nm to 2.0 nm, and there is no obvious correlation between the mean pore radius and the gas breakthrough pressure. However, it is observed that the gas breakthrough

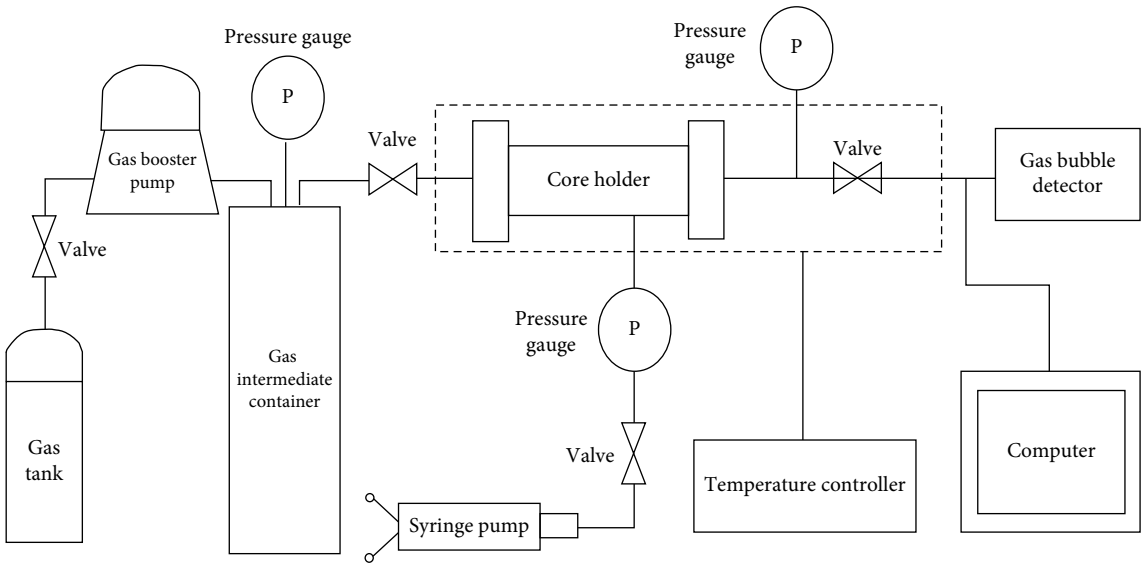

Figure 5: Diagrammatic sketch of the SBS gas breakthrough pressure experiment.

Table 1: Initial pressure difference for cores with different permeability.

Air permeability (Ka) ($10^{-3}\mu m^2$)	Initial pressure difference (MPa)	
	Brined saturated cores	Oil saturated cores
Ka > 0.1	0.1	0.1
0.01 < Ka ≤ 0.1	2.0	0.5
0.001 < Ka ≤ 0.01	5.0	3.0
Ka ≤ 0.001	7.0	5.0

Table 2: Pressure gap and time duration for the breakthrough pressure measurement.

Measurement pressure (Pt) (MPa)	Time duration (minutes)	Pressure gap (MPa)
Pt ≤ 2	30	0.2
2 < Pt ≤ 5	45	0.5
5 < Pt ≤ 10	60	1.0
10 < Pt ≤ 15	90	1.0
Pt > 15	120	1.5

pressure is inversely with the surface area obtained by the BJH theory (S_{BJH}) and the porosity of mesopores obtained by the N_2 adsorption (Figures 6(e) and 6(f)). It indicates that the breakthrough pressure is controlled by the pore radius of macropores, but influenced by the porosity of mesopores. Therefore, the high pressure MIP measurement is enough to determine the gas breakthrough pressure of shales, as long as the correlation functions with the MIP parameters are established.

3.2. Relationship with the Mineral Compositions. Figure 7 gives the relationship between the gas breakthrough pressure and the contents of main minerals and clays. It is clear that the breakthrough pressure is inversely with the content of the quartz, the calcite, and the pyrite, but proportional to the content of the clay and the plagioclase. It can be interpreted that both the quartz and the calcite are brittle minerals and can have significant influence on the development of primary pores and microfractures. The pyrite can be also recognized as the brittle mineral since it is positive to the preservation of the kerogen, yielding more organic pores. Therefore, we define the content of the brittle mineral as the sum of the quartz content, the calcite, and the pyrite content, which can be expressed as,

$$V_{\text{brittle mineral}} = V_{\text{Quartz}} + V_{\text{Calcite}} + V_{\text{Pyrite}}, \quad (1)$$

where V_{Quartz}, V_{Calcite}, and V_{Pyrite} are the content of quartz, the calcite, and the pyrite, respectively.

However, the type of the brittle minerals may be varied in different regions. According to the laboratory tests and literature [48], the simple sum of brittle minerals is not significantly correlated to the mechanical brittleness index. It is recognized that the content of brittle minerals is important for the development of natural and created fractures [49, 50]. Therefore, it reasonable to obtain the relationship that the gas breakthrough pressure is negatively correlated with the content of the brittle minerals.

The fracability index is proportional to the content of the brittle minerals, making it easier for the gas to breakthrough. On the contrary, both the content of the clay and the plagioclase are positively correlated with the breakthrough pressure, implying that the pore volume, pore radius, and the pore connectivity are reduced, and the gas breakthrough capability is then limited. From the application perspective, it is feasible to establish the empirical relationship between the gas breakthrough pressure and the content of the dominant minerals for the well logging calibration. The mineral's profile can be achieved by the quantitative well logging

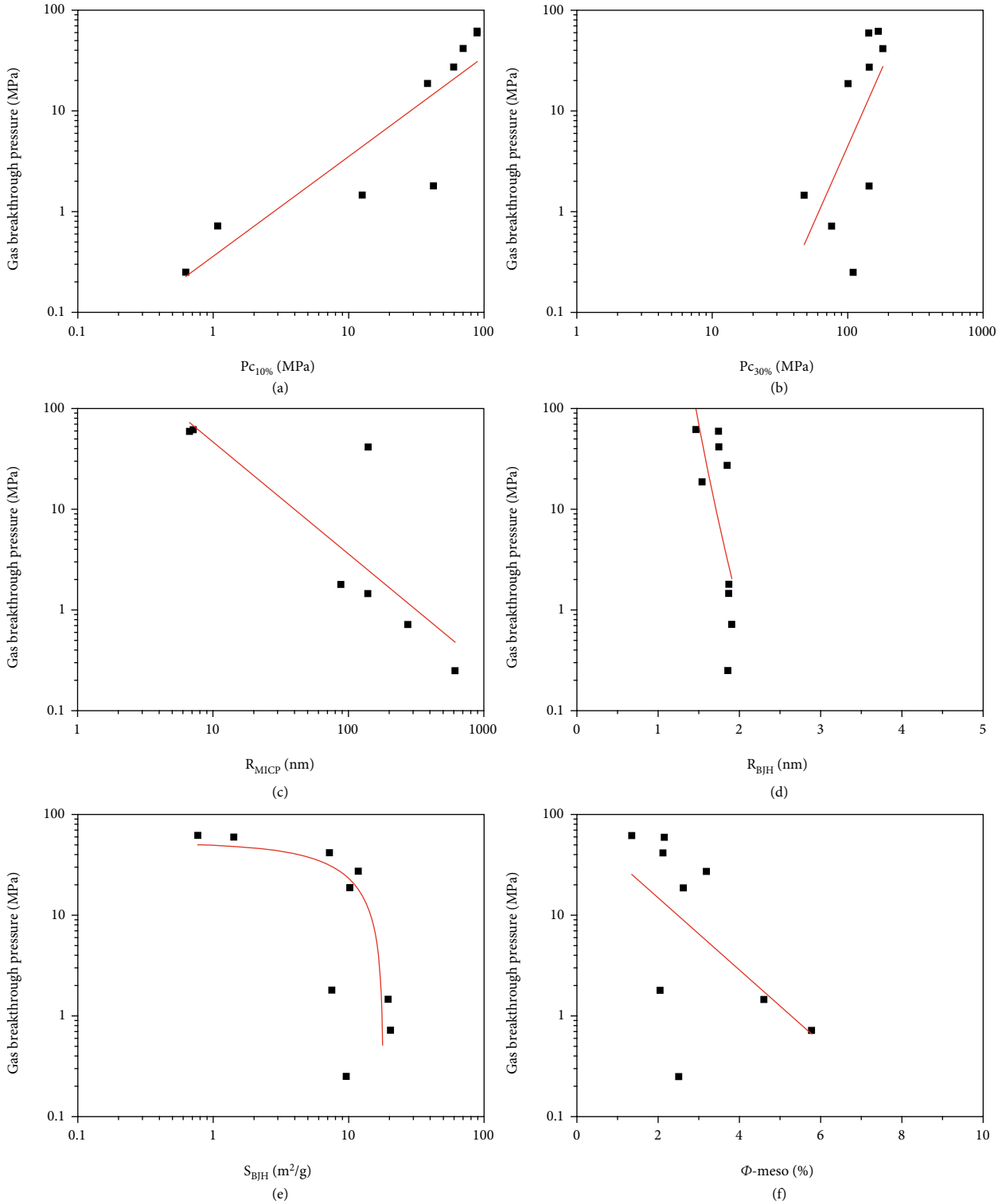

FIGURE 6: Relationships between the gas breakthrough pressure and the pore parameters. (a) The breakthrough pressure and the entry pressure of 10% mercury saturation. (b) The breakthrough pressure and the entry pressure of 30% mercury saturation. (c) The breakthrough pressure and the mean pore radius by MIP. (d) The breakthrough pressure and the mean pore radius by N_2 adsorption. (e) The breakthrough pressure and the mean BJH surface area by N_2 adsorption. (f) The breakthrough pressure and the porosity of mesopores by N_2 adsorption.

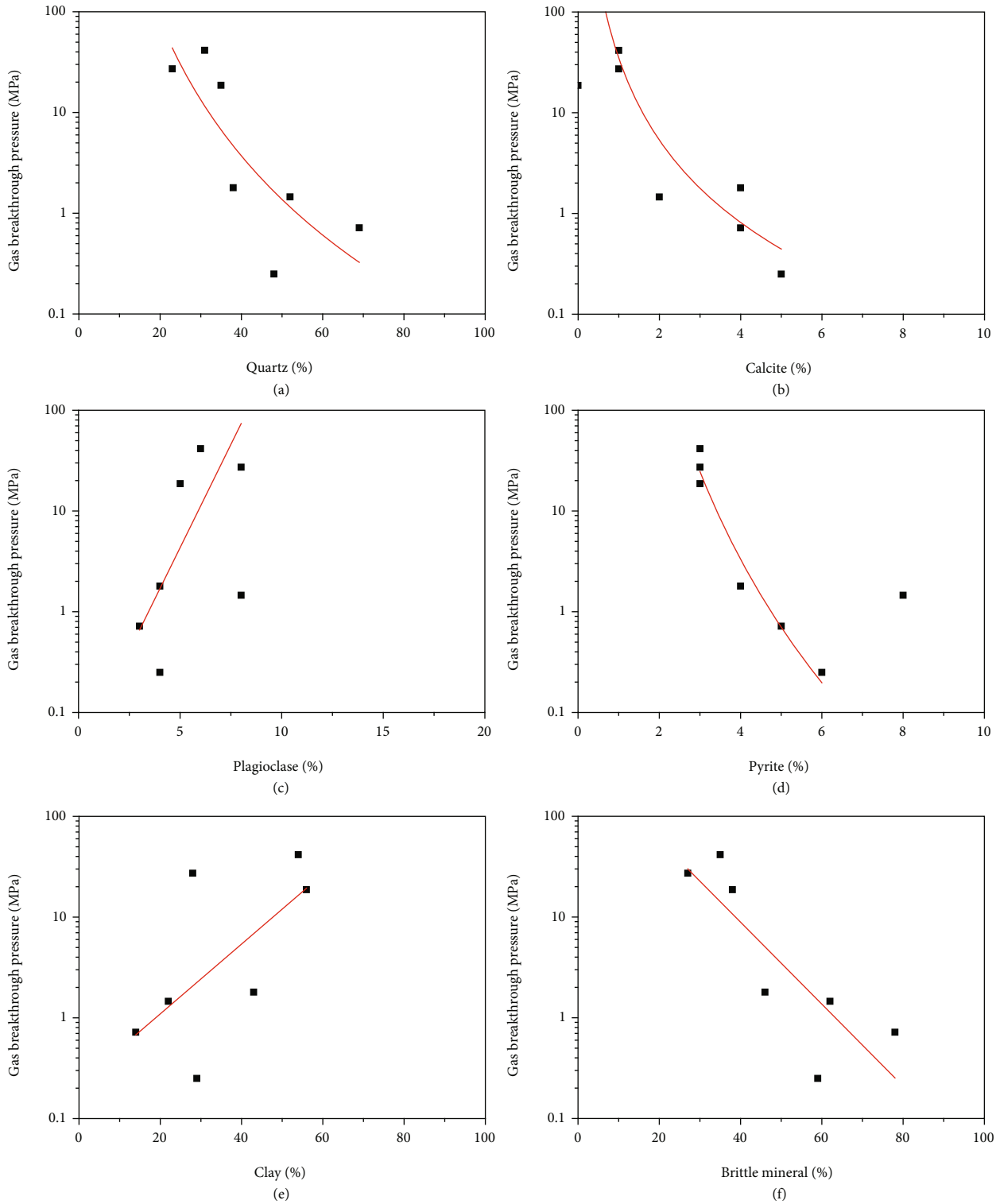

Figure 7: Relationships between the gas breakthrough pressure and the minerals' contents. (a) The quartz content. (b) The calcite content. (c) The plagioclase content. (d) The pyrite content. (e) The clay content. (f) The brittle minerals' contents.

analysis such as the multimineral modeling and the elemental capture spectroscopy (ECS) logging data.

3.3. Relationship with the Geochemical Properties. Figure 8 depicts the relationship between the gas breakthrough pressure and the geochemical parameters obtained by the Rock-Eval pyrolysis. The breakthrough pressure is obviously decreased with the increase of the TOC and the residual carbon content (RC), indicating that the gas is easy to breakthrough in the organic rich formation. The result is similar

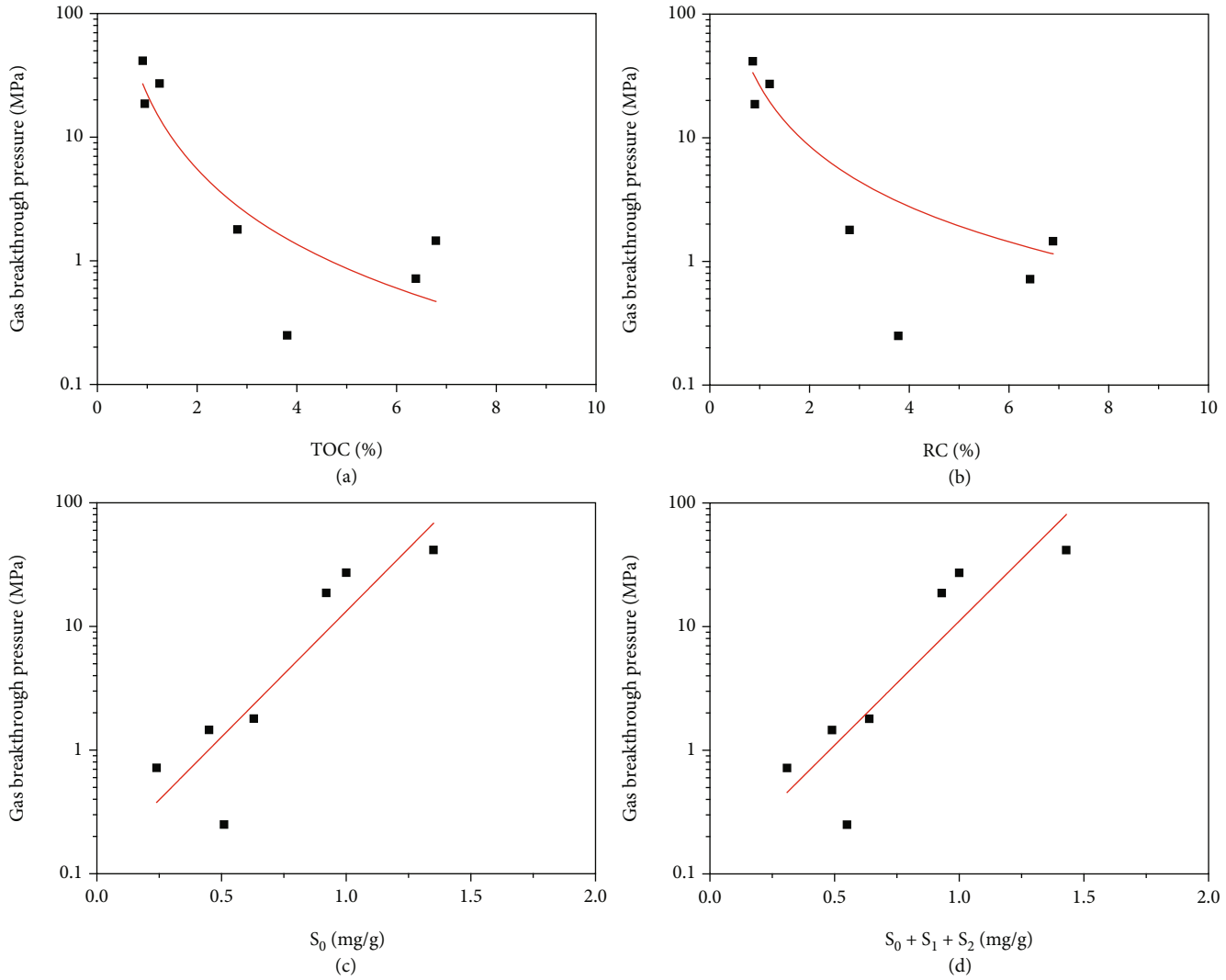

Figure 8: Relationships between the gas breakthrough pressure and the geochemical properties. (a) The total organic carbon content. (b) The residual carbon content. (c) The absorbed free gaseous hydrocarbons. (d) The total amount of the absorbed free gaseous hydrocarbons (S_0), the absorbed free liquid hydrocarbons (S_1), and the residual petroleum potential (S_2).

to the previous publication [3] and revealed that for the unconventional reservoirs such as the gas shale, the shale may not be the good caprock due to the development of micropores, where the methane can be transported and adsorbed in. It is easier for the gas to transport in shales with higher TOC since the organic pores and microfractures are favorable in high TOC shale, improving the gas breakthrough capability. Moreover, the gas breakthrough pressure is positively correlated with the absorbed free gaseous hydrocarbons (S_0), and the total amount of the absorbed free gaseous hydrocarbons (S_0), the absorbed free liquid hydrocarbons (S_1), and the residual petroleum potential (S_2), as shown in Figures 8(c) and 8(d). The result further explained that the quality of the caprock is proportional to the hydrocarbon production index. Reservoirs with larger gas breakthrough pressure can prevent the transportation of the hydrocarbons, yielding higher hydrocarbon contents.

3.4. Implication for the Reservoir Performance. Figures 9(a) and 9(b) show the correlation of the gas breakthrough pressure with the total gas content, and the adsorbed gas content. The total gas content is obtained from the field site desorption data, and the lost gas content is corrected by the USBM (United State Bureau of Mine) method [51, 52]. The adsorbed gas content is measured from the Langmuir fitting of isothermal adsorption experiments. It is clear that the gas breakthrough pressure (Pb) is inversely with both the total gas content and the adsorbed gas content, revealing that the methane is mainly resided in larger pores with smaller breakthrough pressures. Figures 9(c) and 9(d) depict the correlation of the gas breakthrough pressure with porosity and permeability. Similar to conventional reservoirs, the gas is easier to flow in pores with higher porosity and higher permeability. Figure 10(e) gives the relationship between the gas breakthrough pressure and the TOC. It is obvious that the gas breakthrough pressure is inversely with the TOC,

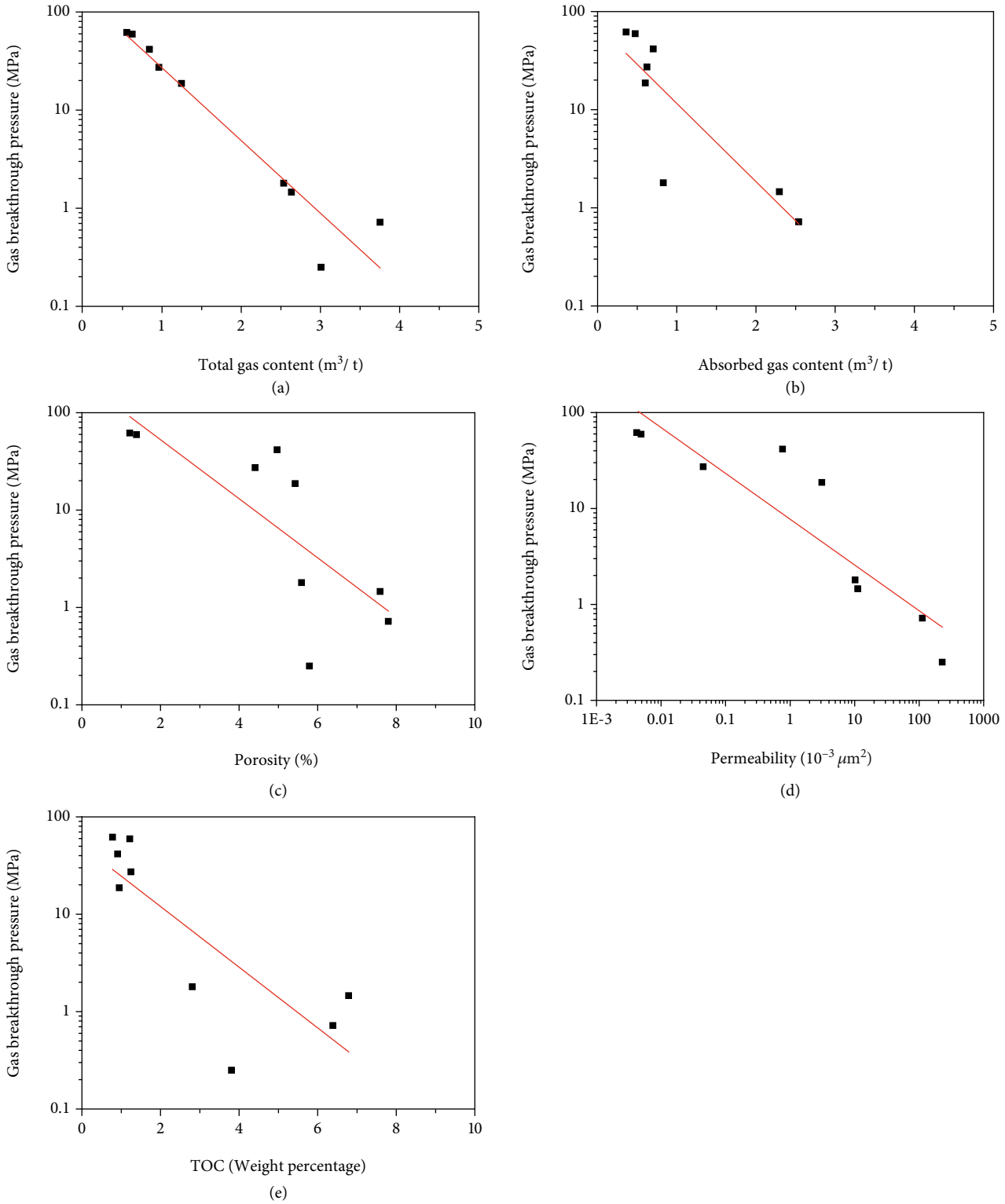

FIGURE 9: Relationships between the gas breakthrough pressure and the reservoir parameters. (a) The total gas content. (b) The adsorbed gas content. (c) The porosity. (d) The permeability. (e) The TOC.

indicating that the organic rich shale cannot have good sealing performance. The possible reason may be that there are large amount of micropores developed in the organic matter. Therefore, the reservoir performance and the favorable gas bearing zones can be inferred from the breakthrough pressure. The sweet spot is assumed to be located in the formation unit where the upper part is composed by the lithology of high breakthrough pressure, low TOC, and low

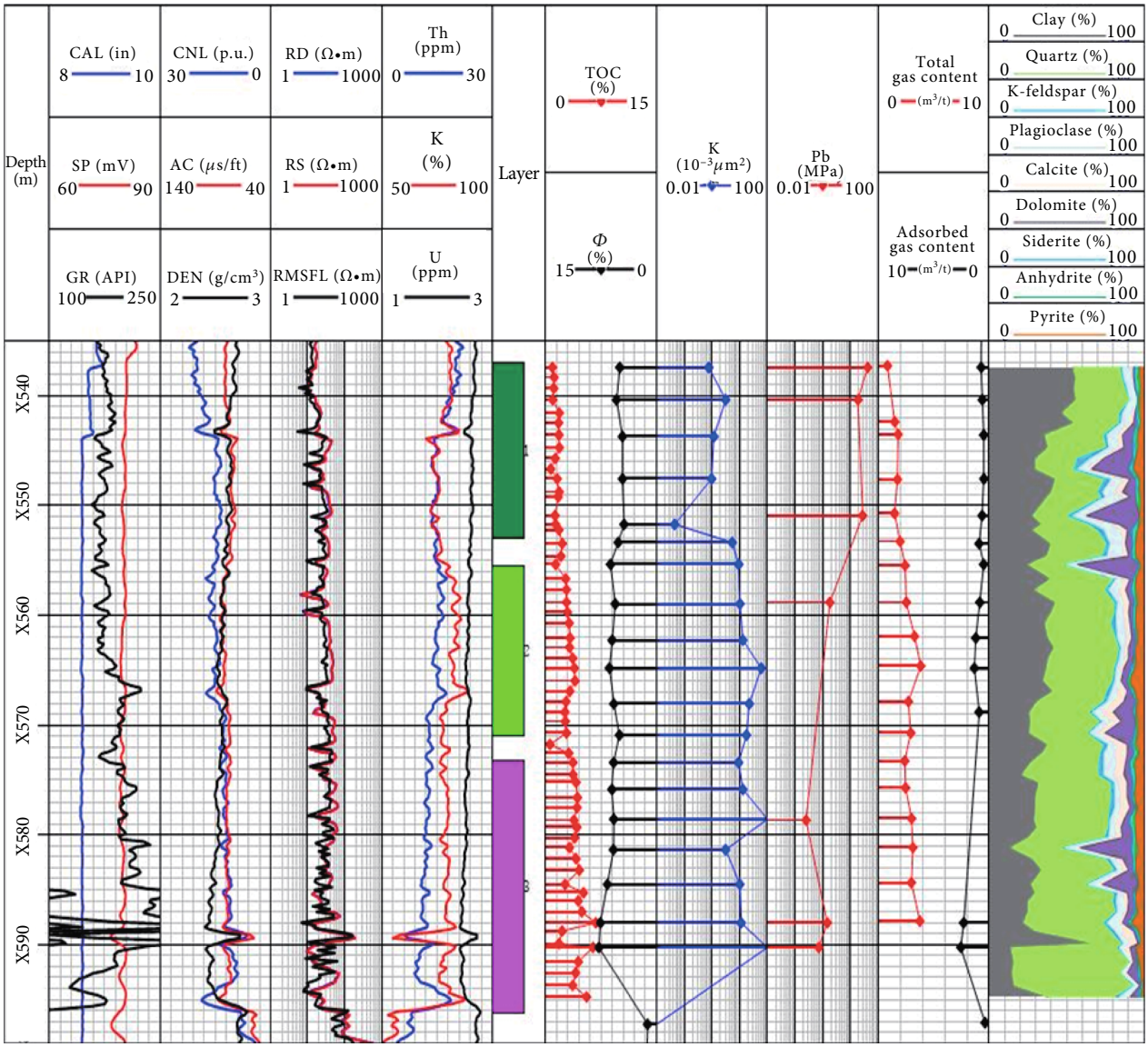

Figure 10: Core and geophysical logging data of the Longmaxi Formation in Y-XX well.

brittle minerals, and the lower part is composed by organic shales of low breakthrough pressure, high TOC, and high brittle minerals.

Figure 10 gives the comprehensive logging responses and corresponding petrophysical, mineralogical, and geochemical data of Y-XX well. Table 3 shows the characteristic values of three gas-bearing layers. It is observed that the upper part is featured as low TOC, low porosity, low quartz content, high breakthrough pressure, and high clay content, whereas the lower part is featured as high TOC, high porosity, high quartz content, low breakthrough pressure, and low clay content. Moreover, it is found that the gamma ray (GR) intensity, the thorium content (Th), and the compensated neutron porosity (CNL) have better gas indication than other conventional geophysical logging responses. The gas rich zone is generally recognized as low breakthrough pressure, showing high GR, low CNL, and low Th. The reservoir quality is improved from the top to the bottom, indicating that the upper part is a promising caprock and the lower part is a favorable sweet spot. The gas breakthrough pressure plays a very important role for the formation evaluation of the gas shale.

4. Discussion

Based on the above analysis, we observed that the gas breakthrough pressure acts as an important role on the reservoir performance. Generally, the sealing capacity of the gas shale is influenced by many factors including the mineralogical compositions, the pore space and its permeability, and the source rock properties. The relationship between the gas breakthrough pressure and the porosity, the pore size, and the permeability can be explained conveniently and behaves the similar law to the conventional reservoir and literatures. However, in our experiments, we did not compare the breakthrough with different measurement methods [23],

Table 3: Geophysical logging and core analysis data of the Longmaxi Formation in Y-XX well.

Layer	1	2	3
Depth (m)	×537-×553	×555.5-×571	×573.2-×596.2
GR (API)	174.5	183.7	207.7
CNL(p.u.)	16.32	15.01	11.95
DEN (g/cm^3)	2.627	2.561	2.506
AC (μs/ft)	76.842	82.017	78.267
RD (Ω.m)	23.57	32.69	38.31
RS (Ω.m)	24.46	33.37	38.45
Th (ppm)	16.32	15.01	11.95
U (ppm)	2.63	2.56	2.51
K (%)	76.84	82.02	78.27
TOC (%)	1.42	3.10	4.16
Pb (MPa)	29.15	1.80	0.81
Φ (%)	4.81	5.76	6.50
Gas content (m^3/t)	1.47	3.06	2.96
Clay (%)	42	35	27
Quartz (%)	32	42	51

which may affect the correlations. In addition, the intrinsic mechanism of the relationships between the gas breakthrough pressure and the mineral composition, the relationships between the gas breakthrough pressure and the source rock property need more data to validate. Due to the lack of experimental data, it is difficult to establish the empirical equation to predict the breakthrough pressure using geophysical logging data. In further study, we will work on more data to verify the result and to generalize the findings for the field application.

5. Conclusion

The paper presents a comprehensive research on the gas breakthrough pressure of shale from the Longmaxi Formation of the A block in the B shale gas field. The influential factors such as mineralogical, petophysical, and geochemical properties are investigated. Moreover, the relationship between the breakthrough pressure and the reservoir quality are discussed. Based on our observations, the main conclusions are as follows:

(1) The breakthrough pressure is inversely with the mean pore radius, and the contents of the brittle minerals such as the quartz and the calcite

(2) The gas is easier to flow and breakthrough in shales of higher TOC due to the development of organic pores in the kerogen and the organic matter

(3) Both the total gas content and the adsorbed gas content are decreased with the breakthrough pressure. The gas breakthrough pressure can be a promising parameter to indicate the sweet spot of unconventional reservoirs

Data Availability

All data analyzed in this study are available from the corresponding authors upon reasonable request.

Conflicts of Interest

The authors declare that they have no conflicts of interest.

Acknowledgments

This work was supported by the National Natural Science Foundation of China (42174142) and the Fundamental Research Funds for the Central Universities (19CX02006A).

References

[1] P. F. Boulin, P. Bretonnier, V. Vassil, A. Samouillet, M. Fleury, and J. M. Lombard, "Sealing efficiency of caprocks: experimental investigation of entry pressure measurement methods," *Marine and Petroleum Geology*, vol. 48, pp. 20–30, 2013.

[2] J. D. Smith, I. Chatzis, and M. A. Ioannidis, "A new technique to measure the breakthrough capillary pressure," *Journal of Canadian Petroleum Technology*, vol. 44, no. 11, pp. 25–31, 2005.

[3] C. Zhang and Q. Yu, "The effect of water saturation on methane breakthrough pressure: an experimental study on the carboniferous shales from the eastern Qaidam Basin, China," *Journal of Hydrology*, vol. 543, no. B, pp. 832–848, 2016.

[4] X. Zhou, X. Lü, H. Quan et al., "Influence factors and an evaluation method about breakthrough pressure of carbonate rocks: an experimental study on the Ordovician of carbonate rock from the Kalpin area, Tarim Basin, China," *Marine and Petroleum Geology*, vol. 104, pp. 313–330, 2019.

[5] L. Cui, W. Ye, Q. Wang, Y. Chen, B. Chen, and Y. J. Cui, "Insights into determination of gas breakthrough in saturated compacted Gaomiaozi bentonite," *Journal of Materials in Civil Engineering*, vol. 32, no. 7, article 04020190, 2020.

[6] R. J. Cuss, J. F. Harrington, D. J. Noy, S. Sathar, and S. Norris, "An experimental study of the flow of gas along synthetic faults of varying orientation to the stress field: implications for performance assessment of radioactive waste disposal," *Journal of Geophysical Research: Solid Earth*, vol. 120, no. 5, pp. 3932–3945, 2015.

[7] C. Galle, "Gas breakthrough pressure in compacted Fo-Ca clay and interfacial gas overpressure in waste disposal context," *Applied Clay Science*, vol. 17, no. 1-2, pp. 85–97, 2000.

[8] Y. Gao, M. Zhao, J. Wang, and C. Zong, "Performance and gas breakthrough during CO_2 immiscible flooding in ultra-low permeability reservoirs," *Petroleum Exploration and Development*, vol. 41, no. 1, pp. 88–95, 2014.

[9] E. J. Guiltinan, D. N. Espinoz, L. P. Cockrell, and M. B. Cardenas, "Textural and compositional controls on mudrock breakthrough pressure and permeability," *Advances in Water Resources*, vol. 121, pp. 162–172, 2018.

[10] S. J. T. Hangx, C. J. Spiers, and C. J. Peach, "Mechanical behavior of anhydrite caprock and implications for CO_2 sealing capacity," *Journal of Geophysical Research*, vol. 15, no. B7, article B07402, 2010.

[11] J. E. Heath, A. T. Dewers, B. J. O. L. McPherson, M. B. Nemer, and P. G. Kotula, "Pore-lining phases and capillary breakthrough pressure of mudstone caprocks: sealing efficiency of geologic CO_2 storage sites," *International Journal of Greenhouse Gas Control*, vol. 11, pp. 204–220, 2012.

[12] S. Kim and J. C. Santamarina, "CO_2 breakthrough and leak-sealing – Experiments on shale and cement," *International Journal of Greenhouse Gas Control*, vol. 19, pp. 471–477, 2013.

[13] Z. Li, M. Dong, S. Li, and S. Huang, "CO_2 sequestration in depleted oil and gas reservoirs– caprock characterization and storage capacity," *Energy Conversion and Management*, vol. 47, no. 11-12, pp. 1372–1382, 2006.

[14] C. W. W. Ng, Z. K. Chen, J. L. Coo, R. Chen, and C. Zhou, "Gas breakthrough and emission through unsaturated compacted clay in landfill final cover," *Waste Management*, vol. 44, pp. 155–163, 2015.

[15] L. Xu, W. M. Ye, Y. G. Chen, B. Chen, and Y. J. Cui, "A new approach for determination of gas breakthrough in saturated materials with low permeability," *Engineering Geology*, vol. 241, pp. 121–131, 2018.

[16] W. M. Ye, Y. J. Cui, L. X. Qian, and B. Chen, "An experimental study of the water transfer through confined compacted GMZ bentonite," *Engineering Geology*, vol. 108, no. 3-4, pp. 169–176, 2009.

[17] Y. Zhao and Q. Yu, "CO_2 breakthrough pressure and permeability for unsaturated low-permeability sandstone of the Ordos Basin," *Journal of Hydrology*, vol. 550, pp. 331–342, 2017.

[18] T. M. Al-Bazali, J. Zhang, M. E. Chenevert, and M. M. Sharma, "Measurement of the sealing capacity of shale caprocks," in *SPE Annual Technical Conference and Exhibition*, Dallas, TX, USA, 2005.

[19] L. Cui, W. Ye, Q. Wang, Y. Chen, B. Chen, and Y. Cui, "Investigation on gas migration in saturated bentonite using the residual capillary pressure technique with consideration of temperature," *Process Safety and Environmental Protection*, vol. 125, pp. 269–278, 2019.

[20] D. N. Espinoza and J. C. Santamarina, "CO_2 breakthrough–caprock sealing efficiency and integrity for carbon geological storage," *International Journal of Greenhouse Gas Control*, vol. 66, pp. 218–229, 2017.

[21] K. Kawaura, K. Akaku, M. Nakano, D. Ito, T. Takahashi, and S. Kiriakehata, "Examination of methods to measure capillary threshold pressures of pelitic rock samples," *Energy Procedia*, vol. 37, pp. 5411–5418, 2013.

[22] M. Sorai, T. Fujii, Y. Kano, S. Uehara, and K. Honda, "Experimental study of sealing performance: effects of particle size and particle-packing state on threshold pressure of sintered compacts," *Journal of Geophysical Research: Solid Earth*, vol. 119, no. 7, pp. 5482–5496, 2014.

[23] T. Wu, Z. Pan, L. D. Connell, B. Liu, X. Fu, and Z. Xue, "Gas breakthrough pressure of tight rocks: a review of experimental methods and data," *Journal of Natural Gas Science and Engineering*, vol. 81, article 103408, 2020.

[24] Y. Deng, S. Chen, X. Pu, and J. Yan, "Characteristics and controlling factors of shale oil reservoir spaces in the Bohai Bay Basin," *Acta Geologica Sinica - English Edition*, vol. 94, no. 2, pp. 253–268, 2020.

[25] Z. Yang, Q. Li, S. Wu, S. Liu, and X. Liu, "Evidence of the near-source accumulation of the tight sandstone gas in northern Ordos basin, north-central China," *Acta Geologica Sinica - English Edition*, vol. 91, no. 5, pp. 1820–1835, 2017.

[26] J. Zhao, Q. Cao, Y. Bai et al., "Petroleum accumulation: from the continuous to discontinuous," *Petroleum Research*, vol. 2, no. 2, pp. 131–145, 2017.

[27] P. J. Armitage, D. R. Faulkner, R. H. Worden, A. C. Aplin, A. R. Butcher, and J. Iliffe, "Experimental measurement of, and controls on, permeability and permeability anisotropy of caprocks from the CO2storage project at the Krechba field, Algeria," *Journal of Geophysical Research*, vol. 116, no. B12, article B12208, 2011.

[28] Y. Chen, "The study and evaluation of the confining behavior of the capping bed by using well logging data," *Geophysical and Geochemical Exploration*, vol. 19, no. 3, pp. 186–194, 1995.

[29] M. J. Rahman, M. Fawad, and N. H. Mondol, "Organic-rich shale caprock properties of potential CO_2 storage sites in the northern North Sea, offshore Norway," *Marine and Petroleum Geology*, vol. 122, article 104665, 2020.

[30] L. K. Thomas, D. L. Katz, and M. R. Tek, "Threshold pressure phenomena in porous media," *SPE Journal*, vol. 243, no. 2, pp. 174–184, 1968.

[31] C. D. Tsakiroglou and M. Fleury, "Resistivity index of fractional wettability porous media," *Journal of Petroleum Science and Engineering*, vol. 22, no. 4, pp. 253–274, 1999.

[32] X.-D. Wang, Z.-X. Jiang, X.-Q. Pang, and J. Zhang, "Comprehensive evaluation of sealing ability of Silurian cap rocks in Talimu Basin," *Journal of Xi'an Shiyou University (Natural Science Edition)*, vol. 19, no. 4, pp. 49–53, 2004.

[33] W. Yan, J. Wang, S. Liu, K. Wang, and Y. Zhou, "Logging identification of the Longmaxi mud shale reservoir in the Jiaoshiba area, Sichuan Basin," *Natural Gas Industry B*, vol. 1, no. 2, pp. 230–236, 2014.

[34] T. Guo and H. Zhang, "Formation and enrichment mode of Jiaoshiba shale gas field, Sichuan Basin," *Petroleum Exploration and Development*, vol. 41, no. 1, pp. 31–40, 2014.

[35] H. Qin, X. Fan, M. Liu, J. Hao, and B. Liang, "Carbon isotope reversal of desorbed gas in Longmaxi shale of Jiaoshiba area, Sicuhan Basin," *Petroleum Research*, vol. 2, no. 2, pp. 169–177, 2017.

[36] F. Yang, S. Xu, F. Hao et al., "Petrophysical characteristics of shales with different lithofacies in Jiaoshiba area, Sichuan Basin, China: implications for shale gas accumulation mechanism," *Marine and Petroleum Geology*, vol. 109, pp. 394–407, 2019.

[37] Z. Fan, J. Hou, X. Ge, P. Zhao, and J. Liu, "Investigating influential factors of the gas absorption capacity in shale reservoirs using integrated petrophysical, mineralogical and geochemical experiments: a case study," *Energies*, vol. 11, no. 11, p. 3078, 2018.

[38] C. Han, G. Liu, C. Ma, M. Qi, Y. Yang, and G. Li, "Influencing factors of shale permeability in the Longmaxi Formation, southern Sichuan Basin and northern YunnanGuizhou depression," *Geofluids*, vol. 2022, Article ID 6832272, 20 pages, 2022.

[39] M. F. Mahmood, Z. Ahmad, and M. Ehsan, "Total organic carbon content and total porosity estimation in unconventional resource play using integrated approach through seismic inversion and well logs analysis within the Talhar shale, Pakistan," *Journal of Natural Gas Science and Engineering*, vol. 52, pp. 13–24, 2018.

[40] Q. Wang, T. Wang, W. Liu et al., "Relationships among composition, porosity and permeability of Longmaxi shale reservoir in the Weiyuan Block, Sichuan Basin, China," *Marine and Petroleum Geology*, vol. 102, pp. 33–47, 2019.

[41] S. Zhang, H. Liu, M. Wang et al., "Shale pore characteristics of Shahejie Formation: implication for pore evolution of shale oil reservoirs in Dongying sag, north China," *Petroleum Research*, vol. 4, no. 2, pp. 113–124, 2019.

[42] A. Hildenbrand, S. Schlomer, and B. M. Krooss, "Gas breakthrough experiments on fine-grained sedimentary rocks," *Geofluids*, vol. 2, no. 1, 2002.

[43] S. Li, M. Dong, Z. Li, S. Huang, H. Qing, and E. Nickel, "Gas breakthrough pressure for hydrocarbon reservoir seal rocks: implications for the security of long-term CO_2 storage in the Weyburn field," *Geofluids*, vol. 5, no. 4, 2005.

[44] C. Zhang and Q. Yu, "Breakthrough pressure and permeability in partially water-saturated shales using methane-carbon dioxide gas mixtures: an experimental study of carboniferous shales from the eastern Qaidam Basin, China," *AAPG Bulletin*, vol. 103, no. 2, pp. 273–301, 2019.

[45] China National Petroleum Company, *SY/T 5748-2013: Determination Method of Gas Breakthrough Pressure in Rock*, Petroleum Industry Press, Beijing, China, 2013.

[46] K. S. W. Sing, D. H. Everett, R. A. W. Haul et al., "Reporting physisorption data for gas/solid systems with special reference to the determination of surface area and porosity," *Pure and Applied Chemistry*, vol. 57, no. 4, pp. 603–619, 1985.

[47] M. Mastalerz, L. Hampton, A. Drobniak, and H. Loope, "Significance of analytical particle size in low-pressure N_2 and CO_2 adsorption of coal and shale," *International Journal of Coal Geology*, vol. 178, pp. 122–131, 2017.

[48] Y. Kang, C. Shang, H. Zhou et al., "Mineralogical brittleness index as a function of weighting brittle minerals– from laboratory tests to case study," *Journal of Natural Gas Science and Engineering*, vol. 77, article 103278, 2020.

[49] C. Zhang and M. Wang, "A critical review of breakthrough pressure for tight rocks and relevant factors," *Journal of Natural Gas Science and Engineering*, vol. 100, article 104456, 2022.

[50] X. Zhou, X. Lü, F. Sui, X. Wang, and Y. Li, "The breakthrough pressure and sealing property of lower Paleozoic carbonate rocks in the Gucheng area of the Tarim Basin," *Journal of Petroleum Science and Engineering*, vol. 208, article 109289, 2022.

[51] W. Dang, J. Zhang, X. Tang et al., "Investigation of gas content of organic-rich shale: a case study from lower Permian shale in southern north China Basin, central China," *Geoscience Frontiers*, vol. 9, no. 2, pp. 559–575, 2018.

[52] W. P. Diamond and S. J. Schatzel, "Measuring the gas content of coal: a review," *International Journal of Coal Geology*, vol. 35, no. 1-4, pp. 311–331, 1998.